Acta Cryst E CRYSTALLOGRAPHIC COMMUNICATIONS

ISSN 2056-9890

The crystal structure of (3*Z*)-4-[(3-hydroxyphenyl)-amino]pent-3-en-2-one: helices and π-stacking interactions of hydrogen-bridged rings

Jebreil Syed and Alen Hadzovic*

Department of Physical and Environmental Sciences, University of Toronto Scarborough, 1065 Military Trail, Toronto, Ontario, M1C 1A4, Canada. *Correspondence e-mail: alen.hadzovic@utoronto.ca

Received 3 March 2026
Accepted 17 April 2026

Edited by J. Ellena, Universidade de São Paulo, Brazil

Keywords: crystal structure; keto–amine; Hirshfeld surface analysis; hydrogen bond; π–π stacking.

CCDC reference: 1818233

Supporting information: this article has supporting information at journals.iucr.org/e

The title compound, $C_{11}H_{13}NO_2$, crystallizes in the monoclinic space group $P2_1/c$ with four molecular units per unit cell and $Z' = 1$. A strong intramolecular N—H···O interaction results in a six-membered hydrogen-bridged ring. An intermolecular O—H···O hydrogen bond leads to a helix formation. The Hirshfeld surface analysis of intermolecular interactions is presented.

1. Chemical context

A direct condensation of acetylacetone (acac) with primary amines or diamines provides a simple route to a broad family of potential coordination ligands (Hernández-Molina & Mederos, 2003). Particularly prominent are the nacnac ligands, in which both carbonyl groups of the keto tautomer are replaced by imine functionalities, for example, in reactions with aniline and its 2,6-dialkyl derivatives (Hadzovic & Song, 2008*a*; Hadzovic & Song, 2008*b*). Also common are the so-called 'half units,' *O*,*N*-donor ligands that retain one unreacted carbonyl group (Hernández-Molina & Mederos, 2003). Designing polydentate systems is straightforward for both nacnacs and half units when the amine component bears additional donor groups.

Despite their structural richness and widespread use in coordination chemistry, the free nacnac and half-unit ligands themselves have received comparatively little crystallographic attention. This contrasts with classical Schiff bases, which require an aryl-substituted carbonyl group and have been extensively analysed for intra- and intermolecular interactions (Dominiak *et al.*, 2003; Karabıyık *et al.*, 2012). To extend similar structural studies to half units and nacnacs, we report here the structure and detailed analysis of the condensation product of acac with one equivalent of 3-aminophenol.

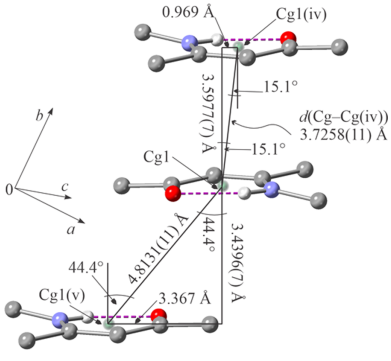

2. Structural commentary

The asymmetric unit of (3*Z*)-4-[(3-hydroxyphenyl)amino]-pent-3-en-2-one (**I**) contains one independent molecule (Fig. 1). The compound, formed through condensation of acetylacetone (acac) and 3-aminophenol, exists as a keto–amine tautomer. Selected bond lengths and angles are provided in Table 1. Atoms O1, C2, C3, C4 and N1 are essentially coplanar (least-squares plane: $-5.1098x + 7.0367y + 1.9389z = 2.6891$, r.m.s. deviation = 0.0195 Å, the furthest atom from the plane is C2 at −0.0315 Å). Methyl atoms C1 and C5 lie −0.169 (2) and 0.0079 (17) Å, respectively, from this plane, while *ipso* atom C6 of the benzene ring

Table 1
Selected geometric parameters (Å, °).

O1—C2	1.2627 (18)	C1—C2	1.503 (2)
N1—C4	1.3352 (19)	C2—C3	1.401 (2)
N1—C6	1.4253 (18)	C3—C4	1.379 (2)
N1—H1N	0.902 (18)	C4—C5	1.495 (2)
C4—N1—H1N	115.6 (11)	C4—C3—C2	125.24 (14)
C6—N1—H1N	116.6 (11)	N1—C4—C3	120.05 (14)
O1—C2—C3	123.26 (13)		

is −0.1980 (16) Å away. The benzene ring is tilted by 20.38 (8)° with respect to the remainder of the molecule.

A six-membered hydrogen-bridged (HB) ring, a quasi-chelate ring that strongly resembles and can act as a covalently formed classical ring (Blagojević *et al.*, 2015), is formed through a strong intramolecular N1—H1N···O1 hydrogen bond (Table 2; for discussion of the remaining hydrogen bonds, see *Supramolecular features*) with $S(6)$ graph-set notation (Etter, 1990). The bond lengths within the six-membered ring (Table 1) lie between typical single and double bonds for all bonding partners (Allen *et al.*, 1987). Together with the bond angles, these values are consistent with a heteroconjugated system and with N1—H1N···O1 as a resonance-assisted hydrogen bond (RAHB; Bertolasi *et al.*, 1995; Filarowski *et al.*, 2005; Steiner, 2002). Elongation of the N1—C6 bond relative to typical N(amine)—C(aromatic) distances (1.355 and 1.394 Å for planar and pyramidal N atoms, respectively; Allen *et al.*, 1987) is also consistent with conjugation of the N-atom lone electron pair within the acac-derived backbone.

The aromaticity of this conjugated system was further assessed using Krygowski's harmonic oscillator measure of aromaticity (HOMA) index (Krygowski, 1993):

$$\mathrm{HOMA} = 1 - \frac{1}{n}\sum \alpha(R_{\mathrm{opt}} - R_{ij})^2$$

where n is the number of bonds, R_{ij} and R_{opt} are experimental and optimal bond lengths, respectively, and α is a dimensionless normalization constant set to give HOMA value of 0 for a non-aromatic system and 1 for a fully aromatic one. Using the bond lengths from Table 1 and literature values for α (CC 257.7, CN 93.52 and CO 157.38; Krygowski, 1993; Krygowski & Cyrański, 2001) and R_{opt} (CC 1.388 Å, CN 1.334 Å and CO 1.265 Å; Krygowski, 1993; Krygowski & Cyrański, 2001) gives HOMA = 0.983, indicating a high level of aromaticity in **I**. In comparison, the HOMA index for acetylacetone is 0.964 based on the single-crystal X-ray analysis data at 210 K from Boese *et al.* (1998).

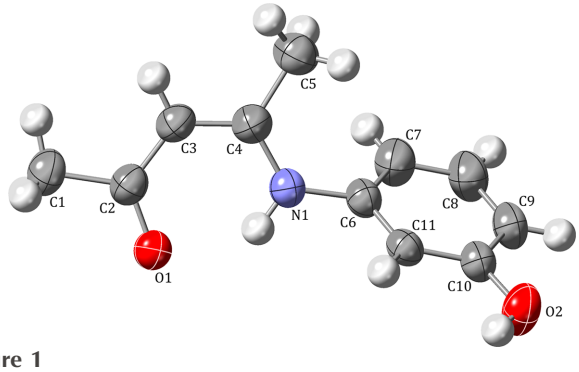

Figure 1
The molecular structure and atom-labeling scheme for **I**, with displacement ellipsoids drawn at the 50% probability level.

Table 2
Hydrogen-bond geometry (Å, °).

D—H···A	D—H	H···A	D···A	D—H···A
N1—H1N···O1	0.903 (18)	1.936 (18)	2.6651 (18)	136.6 (14)
O2—H1O···O1^{i}	0.90 (2)	1.80 (2)	2.6886 (17)	173 (2)
C9—H9···O1^{ii}	0.93	2.65 (2)	3.576 (2)	175 (2)

Symmetry codes: (i) $-x, y+\frac{1}{2}, -z+\frac{1}{2}$; (ii) $-x+1, -y+1, -z+2$.

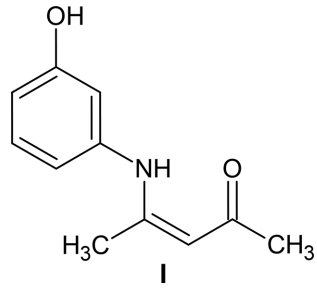

I

3. Supramolecular features

The molecules of **I** link *via* O2—H1O···O1^{i} [symmetry code: (i) $-x, y+\frac{1}{2}, -z+\frac{1}{2}$] intermolecular hydrogen bonds to form helices parallel to the crystallographic b axis [Fig. 2(*a*)], corresponding to a $C(10)$ graph-set assignment (Etter, 1990). The helices wrap around 2_1 screw axes and have two molecules per turn as imposed by symmetry. The left- and right-handed helices, ^{sup}M and ^{sup}P, respectively, interlock in each others grooves, forming a helix layer in the c direction [Fig. 2(*b*)]. There is one contact just below the sum of the van der Waals radii between two interlocked helices: C3···C11^{iii} [symmetry code: (iii) $x, -y+\frac{1}{2}, z-\frac{1}{2}$] at 3.388 (2) Å [purple dotted lines on Fig. 2(*a*) and 3(*a*)]. The helix layers stack along a so that helices of the same handedness lie adjacent to each other, as expected for the space group $P2_1/c$ [Figs. 2(*b*); Miyata *et al.*, 2015]. The only close contact between the layers is a weak C9—H9···O2^{ii} [symmetry code: (ii), $-x+1, -y+1, -z+2$] intermolecular hydrogen bond connecting helices of opposite handedness (Table 2). The geometrical parameters of this interaction are consistent with a hydrogen bond rather than packing effects.

The helix grooves, in which one molecule of **I** 'docks', have an opening of 8.260 (3) Å and are composed of three molecules [Fig. 3(*a*)]. The HB ring docking interactions were analysed using *PLATON* (Spek, 2020) and the findings are summarized in Fig. 3(*b*). The three rings, two from the groove and one from the docking molecule, are stacked in an off-centre antiparallel [α = 0.03 (8)°] fashion and are not equidistant. The $Cg1\cdots Cg1^{iv}$ [symmetry code: (iv) $-x, -y+1, -z+1$] pair displays a short centroid–centroid distance and only minimal lateral displacement, consistent with π–π

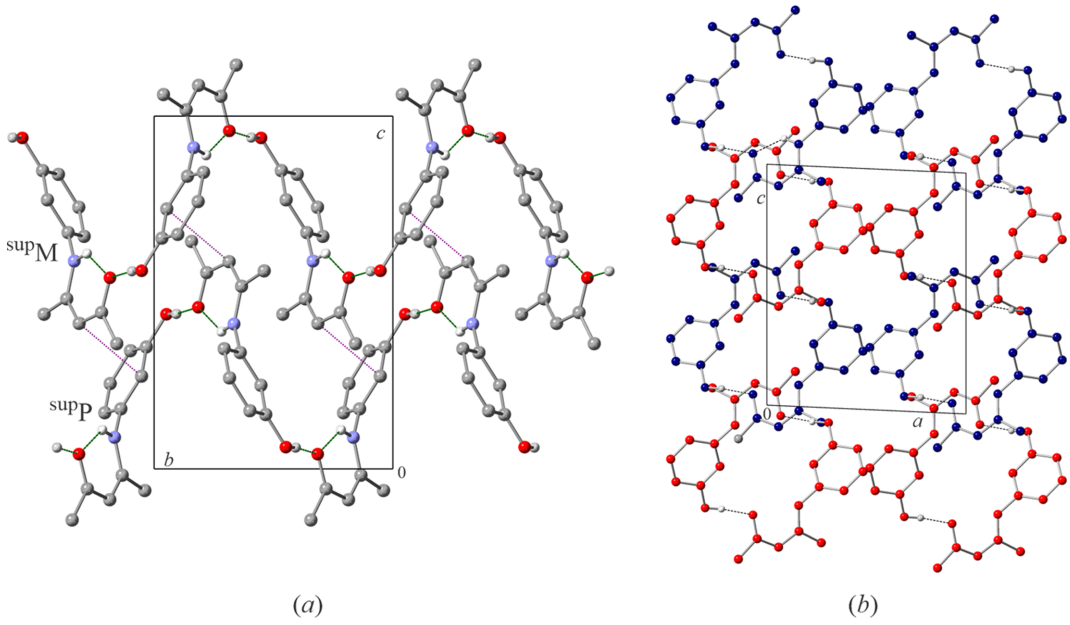

(*a*) (*b*)

Figure 2
Compound **I** forms helices through intramolecular hydrogen bonds, (*a*) viewed along the crystallographic *a* axis, showing both left- and right-handed helices (^{sup}M and ^{sup}P, respectively) and (*b*) viewed along the crystallographic *b* axis emphasizing the packing of helices (blue are left- while red are right-handed). Green dashed lines indicate hydrogen bonds (both intra- and intermolecular), while purple dotted lines show short contacts between the helices.

stacking (Molčanov *et al.*, 2019). Similar parameters have already been reported for the RAHB rings (Blagojević Filipović *et al.*, 2019).

In contrast, although the the second centroid pair, *Cg*1···*Cg*1^{v} [symmetry code: (v) $-x, -y, -z + 1$], has a short interplanar separation [3.4396 (7) Å], its long centroid–centroid distance [4.8131 (11) Å] and substantial slippage (3.367 Å) are not indicative of π–π stacking. Instead, this geometry corresponds to a slipped non-stacking interaction dominated by electrostatic dipole–dipole contributions arising from the interaction between C═O groups. Since carbonyl C atoms are planar (no pyramidalization is observed) and the C2···O1^{v} distance of 3.557 (2) Å is significantly above the 3.22 Å cut-off (Newberry & Raines, 2017), n→π* interactions between C═O groups can be exculded.

There are no significant contacts between benzene rings, with the closest centroid–centroid distance being 5.0134 (11) Å for *Cg*2···*Cg*2^{vi} [symmetry code: (vi) $-x + 1, y - \frac{1}{2}, -z + \frac{3}{2}$].

4. Hirshfeld surface, fingerprint plots and lattice energy

To further analyse the intermolecular interactions in the crystal structure of **I**, the Hirshfeld surface, with different

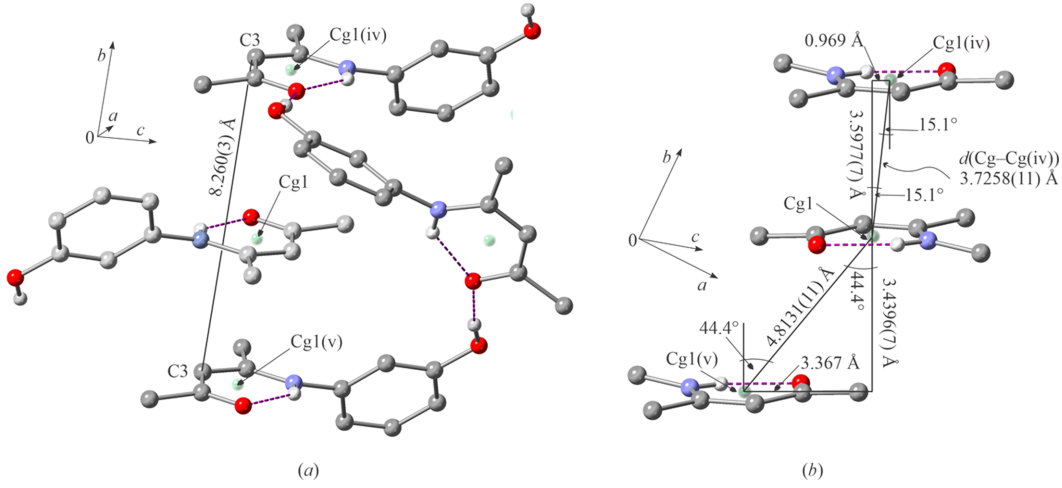

(*a*) (*b*)

Figure 3
Helix groove and docking, showing (*a*) one groove and its docked molecule, with the centroids of the HB rings indicated, and (*b*) centroid–centroid interaction parameters.

functions mapped, and the fingerprint plots were generated using *CrystalExplorer 17.5* (Turner *et al.*, 2017). The fragment patch Hirshfeld surface reveals 16 nearest neighbours for each molecule of **I** (Fig. 4). About 58% of the fragment patch surface belongs to five neighbours: three from the groove (patches 1, 3 and 5) and two from the molecules of the next helix of the opposite handedness (patches 2 and 4), directed along the crystallographic *c* axis. The two hydrogen-bonded molecules of the same helix comprise just under 10% of the surface combined (patches 8 and 9). The remaining nine contacts are distributed among layers along the crystallographic *a* axis.

The d_{norm} Hirshfeld surface [Fig. 5(*a*)], in the standard colour scheme, is dominated by white areas indicative of contacts close to the sum of the van der Waals radii. Two prominent red spots, at keto atom O1 and hydroxyl atom O2, highlight short contacts and coincide with the O—H···O hydrogen bonds within a helix. Less prominent red areas correspond to the C9—H9···O2 contacts between helices of opposite handedness.

In contrast to the relatively featureless d_{norm}, the shape index Hirshfeld surface, *S*, provides significant interaction detail [Fig. 5(*b*)]. The *S* surface reveals 'hollows' (concave red regions) and 'bumps' (convex blue regions) on the surface where neighbouring molecules interlock. A deep concave region at O1 and a high convex region at OH group [dark-red arrows; Fig. 5(*b*)] highlight the strong hydrogen bonds responsible for helix formation [Fig. 5(*c*)]. A similar concave/convex pair is noticeable for the weaker C9—H9···O2 interhelix interactions [dark dashed red arrows of Fig. 5(*b*)]. The bow-tie pattern of green and red/blue triangles [black circle; Fig. 5(*b*)], characteristic of stacking of flat rings and particularly π–π stacking (McKinnon *et al.*, 2004), supports the off-centre π–π stacking for the $Cg1\cdots Cg1^{iv}$ centroid pair [Fig. 5(*d*)]. The black arrows indicate convex regions where the second HB ring, defining $Cg1^{v}$, docks. No bow-tie pattern is observed for these two HB rings. A deep concave region (dashed circle) below the benzene ring arises from interaction with the C5 methyl group from a helix of opposite handedness [Fig. 5(*e*)]. The geometric parameters indicate a weak dispersion C—H···π interaction involving part of the benzene ring, specifically the C8—C9 segment, with a C5—H···C9 distance of 2.871 Å (Nishio, 2011).

The fingerprint plot (Spackman & McKinnon, 2002) (Fig. 6) spans a broad range of d_i and d_e values, from about 1.2 to over 2.4 Å. The colour distribution, with a clear lack of red areas

Fragment Patch		Area /Å²	Area %
No.	Color code		
1		42	17.1
2		30.6	12.5
3		29.2	11.9
4		23.8	9.7
5		17.5	7.1
6		15.3	6.2
7		13.3	5.4
8		12.1	4.9
9		12	4.9
10		8.9	3.6
11		8.8	3.6
12		8.7	3.6
13		8.5	3.5
14		8.2	3.3
15		3	1.2
16		3	1.2

(*a*)

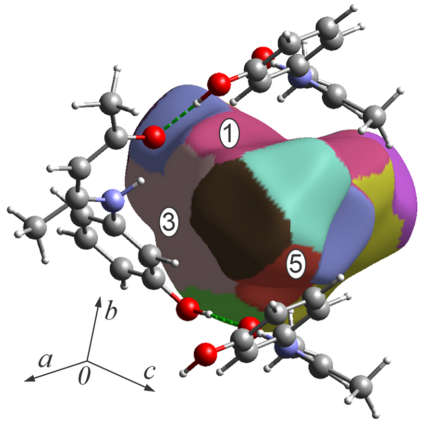

(*b*)

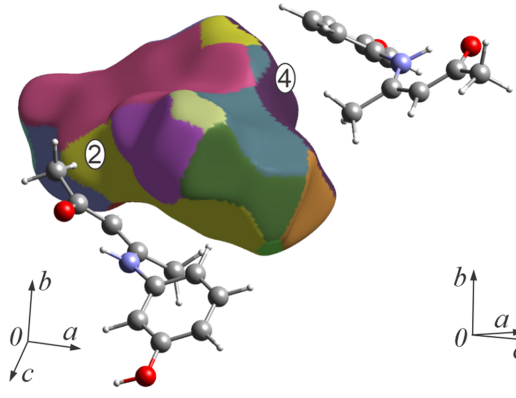

(*c*)

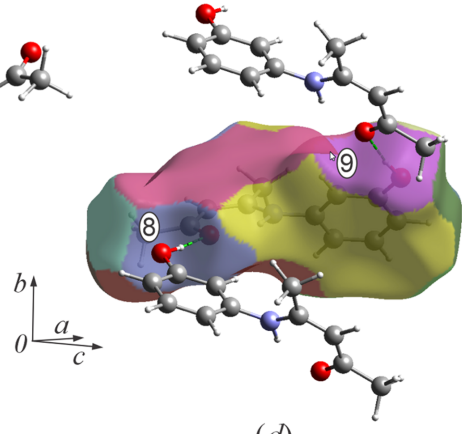

(*d*)

Figure 4
Hirshfeld surface with fragment patch analysis mapped for (*a*) 16 fragments and their contributions to the surface area, (*b*) helix groove contacts and their fragment patches, and (*c*) two large surface and (*d*) fragment patches corresponding to hydrogen bonds within the helix.

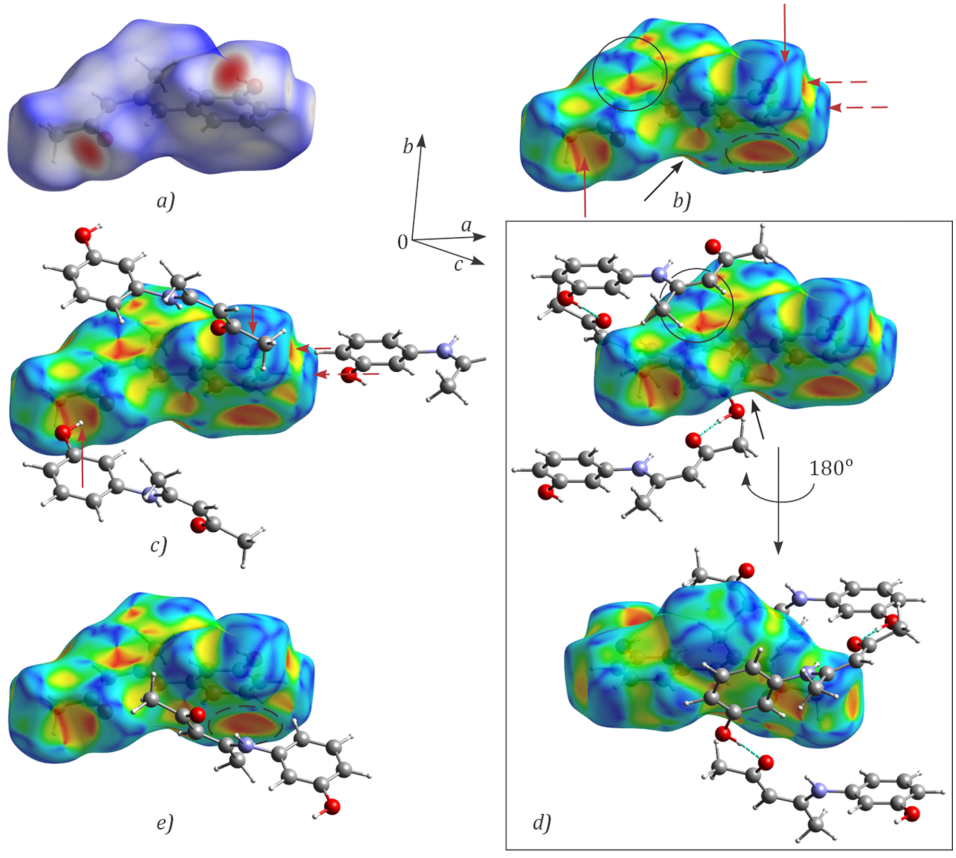

Figure 5
Hirshfeld surfaces, showing (*a*) d_{norm} surface, (*b*) shape index (*S*) surface, (*c*) hydrogen bonding and *S* surface, (*d*) interactions within one helix groove showing π–π interactions between the HB rings and (*e*) C—H$\cdots\pi$ contacts.

indicative of strong dominant interactions, suggests a significant proportion of small but non-zero contacts. The most prominent feature is a two-pronged shape of the plot, typical for hydrogen-bonded systems (McKinnon *et al.*, 2004). Three interactions make up more than 95% of the total: H$\cdots$H, O$\cdots$H and C$\cdots$H (pie chart in Fig. 6). The filtered fingerprint plots and *S* surfaces are shown in Fig. 6. The H$\cdots$H contacts are absent around the HB and benzene rings. The small winged regions (marked with squares) correspond to contacts between molecules of the same helix. A small tip at about 1.2 Å (circle) corresponds to the short contacts between helix layers. The central teal region of the filtered plot is dominated by contacts between stacked helices.

The O$\cdots$H contacts span a broad range of d_i/d_e values and the filtered *S* surface places them predominantly within a single helix. The tips of the two prongs correspond to the closest O—H$\cdots$O contacts. The C$\cdots$H fingerprint plot shows small wings (ellipses), characteristic of C—H$\cdots\pi$ interactions (McKinnon *et al.*, 2004). The tips of these wings correspond to the centre of a deep depression on the *S* surface, seen as a red region near the benzene ring. *PLATON* (Spek, 2020) ring analysis did not reveal any interaction involving the delocalised π-system of the entire benzene ring. A detailed evaluation places the minimum of the concave (red) region around C9 and the corresponding convex (blue) region at H5*C* with points of closest approach of C9$\cdots$H5C^{vi} [symmetry code: (vii) $x, -y+\frac{1}{2}, z+\frac{1}{2}$] = 2.87 Å, C8$\cdots$H5$C^{vi}$ = 3.15 Å and C10$\cdots$H5C^{vii} = 3.08 Å between the helices of the opposite handedness within one helix layer. The remaining important C$\cdots$H contacts form a part of a bow-tie pattern with d_i/d_e values in the range 1.8–2.0 Å. Another part of this pattern appears in the C$\cdots$C interactions and lies in the teal-coloured region of the fingerprint plot. The tip of the plot corresponds to the short C3$\cdots$C11^{iii} contact and appears as a small green patch on the corresponding Hirshfeld surface. Although they represent less than 2% of all contacts, O$\cdots$C and N$\cdots$C contacts complete the bow-tie pattern associated with HB ring stacking and are therefore essential for understanding the ring interactions.

The CE-B3LYP/6-31G(d,p) lattice energy, E_{latt} (Turner *et al.*, 2014), converged at -140 kJ mol^{-1} [Fig. 7(*a*)]. The principal contributor to E_{latt} is the dispersion term at -107.1 kJ mol^{-1}, followed by the electrostatic and polarization terms at -90.16 and -18.35 kJ mol^{-1}, respectively. The repulsion–exchange term destabilizes the lattice by +75.9 kJ mol^{-1}.

The energy framework diagrams (Mackenzie *et al.*, 2017) show that the bulk of the Coulombic forces occur within a single helix [Fig. 7(*d*)], while the dispersion is almost equally distributed throughout the lattice but is somewhat stronger between interlocking helices [Fig. 7(*c*)], consistent with

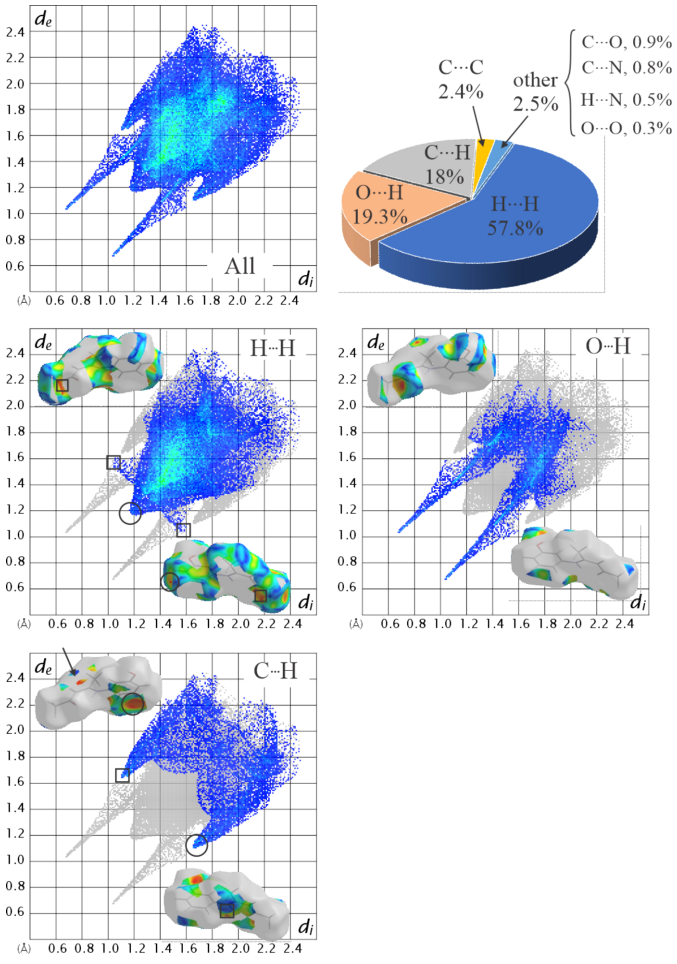

Figure 6
Distribution of contacts and fingerprint plots for **I**.

previous findings on π-stacking (Molčanov *et al.*, 2019). As the annotated energies indicate, the strongest interacting is the pair of two hydrogen-bonded molecules within a helix followed by the interactions within the helix grove [Fig. 7(*e*)].

5. Database survey

A search of the Cambridge Structural Database (CSD, Version 5.44, April 2023 update; Groom *et al.*, 2016) targeting structures derived from the condensation of acetylacetone and an aromatic amine provided 91 results (organic structures only). The closest relative to compound **I** is 4-[(2-hydroxyphenyl)amino]pent-3-en-2-one, the keto–imine derived from the condensation of acetylacetone and 2-aminophenol. There are six deposits for this compound (all orthorhombic, space group $P2_12_12_1$): CSD refcodes MEHTEY (Kabak *et al.*, 1998), MEHTEY1 (Chen *et al.*, 1999), MEHTEY2 (Rajnikant *et al.*, 2006), MEHTEY3 (Basu *et al.*, 2010), MEHTEY4 (Fatiha *et al.*, 2012) and MEHTEY5 (Salehi *et al.*, 2012). Intermolecular hydrogen bonding (also producing helical supramolecular structure) has been discussed briefly in all cases. Salehi *et al.* (2012) also include a brief discussion on resonance-assisted hydrogen bonds.

Table 3
Experimental details.

Crystal data	
Chemical formula	$C_{11}H_{13}NO_2$
M_r	191.22
Crystal system, space group	Monoclinic, $P2_1/c$
Temperature (K)	295
a, b, c (Å)	10.109 (1), 8.2598 (8), 12.2074 (13)
β (°)	92.539 (4)
V (Å^3)	1018.30 (18)
Z	4
Radiation type	Mo $K\alpha$
μ (mm^{-1})	0.09
Crystal size (mm)	0.39 × 0.32 × 0.09
Data collection	
Diffractometer	Bruker SMART X2S
Absorption correction	Multi-scan (*SADABS*; Bruker, 2004)
No. of measured, independent and observed [$I > 2\sigma(I)$] reflections	12414, 2304, 1661
R_{int}	0.037
$(\sin\theta/\lambda)_{max}$ (Å^{-1})	0.649
Refinement	
$R[F^2 > 2\sigma(F^2)]$, $wR(F^2)$, S	0.043, 0.131, 1.05
No. of reflections	2304
No. of parameters	135
H-atom treatment	H atoms treated by a mixture of independent and constrained refinement
$\Delta\rho_{max}$, $\Delta\rho_{min}$ (e Å^{-3})	0.16, −0.17

Computer programs: *XPREP* (Bruker, 2004), *SAINT* (Bruker, 2004) and *SHELXL2019* (Lübben *et al.*, 2019).

6. Synthesis and crystallization

Acetylacetone (2.3 mmol, 2.3 ml) was added dropwise to a stirred solution of 3-aminophenol (2.3 mmol, 0.25 g) in 95% ethanol (10 ml). The reaction was stirred at ambient temperature for 45 min, covered and then left to stand. After two days, colourless crystals were collected giving an 88% yield (1.8 g) of the title compound.

6.1. Analytical data

^{1}H NMR ($CHCl_3$, δ from TMS): 2.08 (*s*, 3H, –CH_3), 2.14 (*s*, 3H, –CH_3), 5.20 (*s*, 1H, CH), ^{13}C NMR ($CHCl_3$, δ from TMS): 20.16, 28.46 (–CH_3), 97.5 (CH, acac backbone), 111.5, 114.2, 115.7, 130.6, 138.8, 158.67 (benzene ring carbons), 163.0 (CN) and 169.1 (CO). Elemental analysis calculated (%) for $C_{11}H_{13}NO_2$: C 69.09, N 7.32; found: C 69.07, N 7.56. MS–ESI: 190.097 (base peak, $M - H^+$), 148.038 $[M - C(=O)CH_3]^{\cdot -}$.

7. Refinement

Crystal data, data collection and structure refinement details are summarized in Table 3. The positional parameters of the H atoms bonded to N1 and O2, *i.e.* H1*N* and H1*O*, were refined while their displacement parameters were constrained in the usual manner. See the figures in the supporting information for the residual electron-density maps before and after the refinement of atoms H1*N* and H1*O*.

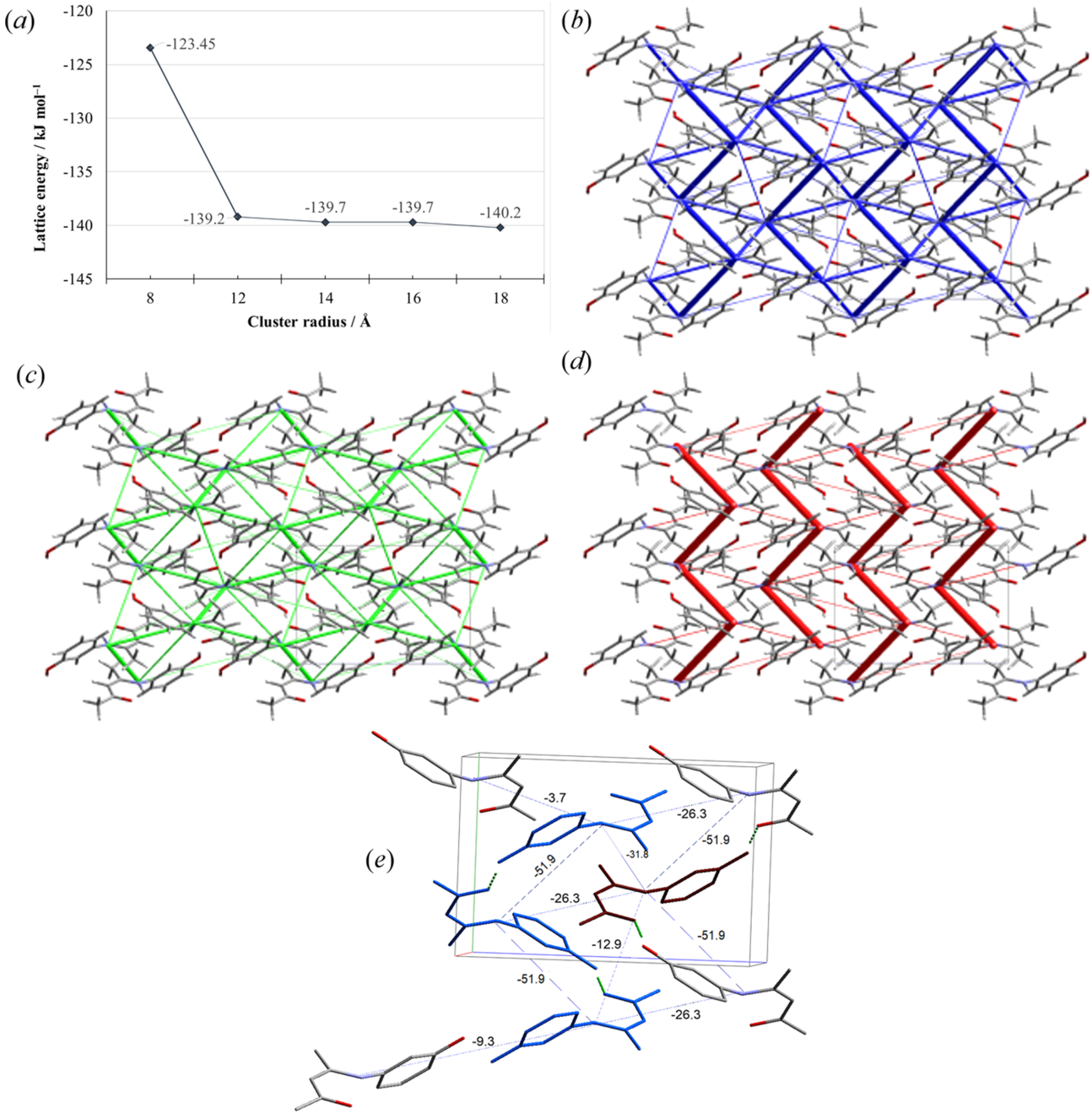

Figure 7
(*a*) Lattice energy convergence plot and (*b*) total energy, (*c*) dispersion, (*d*) Coulombic and (*e*) annotated total energy framework diagrams calculated using the CE-B3LYP/6-31G(p,d) benchmark electron-density model. The tube size is set at 40, and the energy cut-off at 3.00 kJ mol^{-1} for all framework diagrams. All diagrams are viewed along the crystallographic *a* axis.

Acknowledgements

This work is a part of the fourth year undergraduate research thesis (by JS) and is entirely funded from the undergraduate budget of Department of Physical and Environmental Sciences, University of Toronto Scarborough, which the authors gratefully acknowledge. Special thanks go to Mr Tony Adamo, manager of the TRACES facility at our department for providing MS spectra and elemental analysis results, and Dr Scott Ballantyne, senior manager (finance and operations) for his assistance in procuring materials. Funding for this research was provided by the Department of Physical and Environmental Sciences, University of Toronto Scarborough.

References

Allen, F. H., Kennard, O., Watson, D. G., Brammer, L., Orpen, A. G. & Taylor, R. (1987). *J. Chem. Soc. Perkin Trans. 2* pp. S1–19.
Basu, S., Gupta, G., Das, B. & Rao, K. M. (2010). *J. Organomet. Chem.* **695**, 2098–2104.
Bertolasi, V., Gilli, P., Ferretti, V. & Gilli, G. (1995). *Acta Cryst.* B**51**, 1004–1015.

Blagojević, J. P. & Zarić, S. D. (2015). *Chem. Commun.* **51**, 12989–12991.
Blagojević Filipović, J. P., Hall, M. B. & Zarić, S. D. (2019). *Cryst. Growth Des.* **19**, 5619–5628.
Boese, R., Antipin, M. Yu., Bläser, D. & Lyssenko, K. A. (1998). *J. Phys. Chem. B* **102**, 8654–8660.
Bruker (2004). *SAINT*, *XPREP* and *SADABS*. Bruker AXS Inc., Madison, Wisconsin, USA.
Chen, Z.-F., Li, S.-T., Wang, X.-J., Hu, R.-X., Liang, H. & Yu, K.-B. (1999). *Chin. J. Org. Chem.* **19**, 513.
Dominiak, P. M., Grech, E., Barr, G., Teat, S., Mallinson, P. & Woźniak, K. (2003). *Chem. A Eur. J.* **9**, 963–970.
Etter, M. S. (1990). *Acc. Chem. Res.* **23**, 120–126.
Fatiha, B., Saida, K., Safia, C., Ali, O. & Lydia, B. (2012). *Acta Cryst.* E**68**, o2188–o2189.
Filarowski, A., Kochel, A., Cieslik, K. & Koll, A. (2005). *J. Phys. Org. Chem.* **18**, 986–993.
Groom, C. R., Bruno, I. J., Lightfoot, M. P. & Ward, S. C. (2016). *Acta Cryst.* B**72**, 171–179.
Hadzovic, A. & Song, D. (2008*a*). *Organometallics* **27**, 1290–1298.
Hadzovic, A. & Song, D. (2008*b*). *Inorg. Chem.* **47**, 12010–12017.
Hernández-Molina, R. & Mederos, A. (2003). *Acyclic and Macrocyclic Schiff Base Ligands* in *Comprehensive Coordination Chemistry II*, edited by J. A. McCleverty & T. J. Meyer, pp. 411–446. Oxford: Pergamon Press.
Kabak, M., Elmali, A. & Elerman, Y. (1998). *J. Mol. Struct.* **470**, 295–300.
Karabıyık, H., Karabıyık, H. & Ocak İskeleli, N. (2012). *Acta Cryst.* B**68**, 71–79.
Krygowski, T. M. (1993). *J. Chem. Inf. Comput. Sci.* **33**, 70–78.
Krygowski, T. M. & Cyrański, M. K. (2001). *Chem. Rev.* **101**, 1385–1420.
Lübben, J., Wandtke, C. M., Hübschle, C. B., Ruf, M., Sheldrick, G. M. & Dittrich, B. (2019). *Acta Cryst.* A**75**, 50–62.
Mackenzie, C. F., Spackman, P. R., Jayatilaka, D. & Spackman, M. A. (2017). *IUCrJ* **4**, 575–587.
McKinnon, J. J., Spackman, M. A. & Mitchell, A. S. (2004). *Acta Cryst.* B**60**, 627–668.
Miyata, M., Tohnai, N., Hisaki, I. & Sasaki, T. (2015). *Symmetry* **7**, 1914–1928.
Molčanov, K., Milašinović, V. & Kojić-Prodić, B. (2019). *Cryst. Growth Des.* **19**, 5967–5980.
Newberry, R. W. & Raines, R. T. (2017). *Acc. Chem. Res.* **50**, 1838–1846.
Nishio, M. (2011). *Phys. Chem. Chem. Phys.* **13**, 13873–13900.
Rajnikant, D., Dinesh, , Kamni, , Kanwal, P., Purohit, D. H., Joshi, M. J., Parekh, B. & Joshi, M. J. (2006). *Heterocycl. Commun.* **12**, 129–134.
Salehi, M., Dutkiewicz, G., Rezaei, A., Amoozadeh, A., Rahmani, S., Grivani, G. H. & Kubicki, M. (2012). *J. Chem. Crystallogr.* **42**, 871–878.
Spackman, M. A. & McKinnon, J. J. (2002). *CrystEngComm* **4**, 378–392.
Spek, A. L. (2020). *Acta Cryst.* E**76**, 1–11.
Steiner, T. (2002). *Angew. Chem. Int. Ed.* **41**, 48–76.
Turner, M. J., Grabowsky, S., Jayatilaka, D. & Spackman, M. A. (2014). *J. Phys. Chem. Lett.* **5**, 4249–4255.
Turner, M. J., McKinnon, J. J., Wolff, S. K., Grimwood, D. J., Spackman, P. R., Jayatilaka, D. & Spackman, M. A. (2017). *CrystalExplorer17*. University of Western Australia. https://hirshfeldsurface.net.

supporting information

Acta Cryst. (2026). E**82** [https://doi.org/10.1107/S2056989026004068]

The crystal structure of (3*Z*)-4-[(3-hydroxyphenyl)amino]pent-3-en-2-one: helices and π-stacking interactions of hydrogen-bridged rings

Jebreil Syed and Alen Hadzovic

Computing details

(3*Z*)-4-[(3-Hydroxyphenyl)amino]pent-3-en-2-one

Crystal data

$C_{11}H_{13}NO_2$
M_r = 191.22
Monoclinic, $P2_1/c$
a = 10.109 (1) Å
b = 8.2598 (8) Å
c = 12.2074 (13) Å
β = 92.539 (4)°
V = 1018.30 (18) Å^3
Z = 4
$F(000)$ = 408
D_x = 1.247 Mg m^{-3}
Mo $K\alpha$ radiation, λ = 0.71073 Å
Cell parameters from 3910 reflections
θ = 3.0–25.5°
μ = 0.09 mm^{-1}
T = 295 K
Prism, white
0.39 × 0.32 × 0.09 mm

Data collection

Bruker SMART X2S diffractometer
$\theta/2\theta$ scans
Absorption correction: multi-scan (SADABS; Bruker, 2004)
12414 measured reflections
2304 independent reflections
1661 reflections with $I > 2\sigma(I)$
R_{int} = 0.037
θ_{max} = 27.5°, θ_{min} = 2.0°
h = −13→12
k = −10→8
l = −15→15

Refinement

Refinement on F^2
Least-squares matrix: full
$R[F^2 > 2\sigma(F^2)]$ = 0.043
$wR(F^2)$ = 0.131
S = 1.05
2304 reflections
135 parameters
0 restraints
Hydrogen site location: mixed
H atoms treated by a mixture of independent and constrained refinement
$w = 1/[\sigma^2(F_o^2) + (0.0587P)^2 + 0.1926P]$ where $P = (F_o^2 + 2F_c^2)/3$
$(\Delta/\sigma)_{max}$ = 0.001
$\Delta\rho_{max}$ = 0.16 e Å^{-3}
$\Delta\rho_{min}$ = −0.17 e Å^{-3}

Special details

Geometry. All esds (except the esd in the dihedral angle between two l.s. planes) are estimated using the full covariance matrix. The cell esds are taken into account individually in the estimation of esds in distances, angles and torsion angles; correlations between esds in cell parameters are only used when they are defined by crystal symmetry. An approximate (isotropic) treatment of cell esds is used for estimating esds involving l.s. planes.

Fractional atomic coordinates and isotropic or equivalent isotropic displacement parameters (Å²)

	x	*y*	*z*	U_{iso}*/U_{eq}
O1	0.43035 (10)	0.81490 (15)	0.54180 (8)	0.0599 (3)
O2	0.81010 (12)	0.44803 (18)	0.93832 (10)	0.0748 (4)
H1O	0.728 (2)	0.407 (3)	0.9392 (16)	0.090*
N1	0.65951 (13)	0.66563 (17)	0.58920 (10)	0.0518 (3)
H1N	0.5874 (18)	0.719 (2)	0.6112 (13)	0.062*
C1	0.35690 (18)	0.8435 (2)	0.35503 (14)	0.0701 (5)
H1A	0.390076	0.818741	0.284480	0.105*
H2A	0.348530	0.958690	0.362603	0.105*
H3A	0.271802	0.793723	0.361572	0.105*
C2	0.45131 (14)	0.77987 (19)	0.44339 (12)	0.0507 (4)
C3	0.55872 (15)	0.68582 (19)	0.41245 (12)	0.0512 (4)
H3	0.561171	0.656140	0.339084	0.061*
C4	0.66112 (14)	0.63373 (18)	0.48205 (12)	0.0486 (4)
C5	0.77347 (17)	0.5391 (2)	0.43852 (15)	0.0674 (5)
H5A	0.743665	0.482666	0.373259	0.101*
H5B	0.804881	0.462392	0.492717	0.101*
H5C	0.843976	0.611567	0.421641	0.101*
C6	0.76327 (14)	0.63947 (19)	0.67015 (12)	0.0477 (4)
C7	0.88744 (15)	0.7068 (2)	0.65909 (15)	0.0627 (5)
H7	0.906071	0.766290	0.596935	0.075*
C8	0.98306 (15)	0.6842 (2)	0.74194 (15)	0.0642 (5)
H8	1.067104	0.727533	0.734505	0.077*
C9	0.95668 (14)	0.5991 (2)	0.83511 (14)	0.0566 (4)
H9	1.021965	0.586059	0.890515	0.068*
C10	0.83197 (14)	0.53259 (19)	0.84595 (13)	0.0494 (4)
C11	0.73545 (13)	0.55284 (18)	0.76281 (12)	0.0461 (4)
H11	0.651851	0.507906	0.769582	0.055*

Atomic displacement parameters (Å²)

	U^{11}	U^{22}	U^{33}	U^{12}	U^{13}	U^{23}
O1	0.0502 (6)	0.0799 (8)	0.0490 (6)	0.0070 (5)	−0.0035 (5)	−0.0044 (5)
O2	0.0536 (7)	0.1028 (11)	0.0667 (8)	−0.0156 (7)	−0.0118 (6)	0.0267 (7)
N1	0.0422 (6)	0.0632 (8)	0.0497 (7)	0.0027 (6)	−0.0027 (5)	−0.0012 (6)
C1	0.0693 (11)	0.0823 (13)	0.0570 (10)	0.0084 (9)	−0.0150 (8)	−0.0004 (9)
C2	0.0476 (8)	0.0552 (9)	0.0487 (8)	−0.0089 (7)	−0.0037 (6)	0.0023 (7)
C3	0.0526 (8)	0.0576 (10)	0.0433 (8)	−0.0071 (7)	0.0008 (6)	−0.0004 (7)
C4	0.0482 (8)	0.0473 (8)	0.0506 (8)	−0.0085 (6)	0.0035 (6)	0.0008 (7)
C5	0.0629 (10)	0.0683 (11)	0.0715 (11)	0.0053 (9)	0.0076 (8)	−0.0079 (9)
C6	0.0413 (7)	0.0477 (8)	0.0535 (8)	0.0018 (6)	−0.0041 (6)	−0.0034 (7)
C7	0.0510 (9)	0.0659 (11)	0.0706 (11)	−0.0122 (8)	−0.0031 (7)	0.0138 (8)
C8	0.0415 (8)	0.0670 (11)	0.0832 (12)	−0.0123 (7)	−0.0069 (8)	0.0117 (9)
C9	0.0407 (7)	0.0571 (10)	0.0707 (10)	0.0001 (7)	−0.0119 (7)	0.0022 (8)
C10	0.0430 (7)	0.0498 (9)	0.0550 (8)	0.0017 (6)	−0.0028 (6)	0.0013 (7)
C11	0.0350 (6)	0.0490 (8)	0.0541 (8)	−0.0020 (6)	0.0007 (6)	−0.0054 (7)

Geometric parameters (Å, º)

O1—C2	1.2627 (18)	C5—H5A	0.9600
O2—C10	1.3528 (19)	C5—H5B	0.9600
O2—H1O	0.89 (2)	C5—H5C	0.9600
N1—C4	1.3352 (19)	C6—C11	1.378 (2)
N1—C6	1.4253 (18)	C6—C7	1.385 (2)
N1—H1N	0.902 (18)	C7—C8	1.380 (2)
C1—C2	1.503 (2)	C7—H7	0.9300
C1—H1A	0.9600	C8—C9	1.374 (2)
C1—H2A	0.9600	C8—H8	0.9300
C1—H3A	0.9600	C9—C10	1.387 (2)
C2—C3	1.401 (2)	C9—H9	0.9300
C3—C4	1.379 (2)	C10—C11	1.3865 (19)
C3—H3	0.9300	C11—H11	0.9300
C4—C5	1.495 (2)		
C10—O2—H1O	113.0 (13)	C4—C5—H5C	109.5
C4—N1—C6	127.50 (14)	H5A—C5—H5C	109.5
C4—N1—H1N	115.6 (11)	H5B—C5—H5C	109.5
C6—N1—H1N	116.6 (11)	C11—C6—C7	120.49 (13)
C2—C1—H1A	109.5	C11—C6—N1	118.50 (13)
C2—C1—H2A	109.5	C7—C6—N1	120.92 (14)
H1A—C1—H2A	109.5	C8—C7—C6	118.84 (16)
C2—C1—H3A	109.5	C8—C7—H7	120.6
H1A—C1—H3A	109.5	C6—C7—H7	120.6
H2A—C1—H3A	109.5	C9—C8—C7	121.38 (15)
O1—C2—C3	123.26 (13)	C9—C8—H8	119.3
O1—C2—C1	118.34 (15)	C7—C8—H8	119.3
C3—C2—C1	118.40 (14)	C8—C9—C10	119.50 (14)
C4—C3—C2	125.24 (14)	C8—C9—H9	120.3
C4—C3—H3	117.4	C10—C9—H9	120.3
C2—C3—H3	117.4	O2—C10—C11	122.46 (13)
N1—C4—C3	120.05 (14)	O2—C10—C9	117.82 (13)
N1—C4—C5	119.58 (14)	C11—C10—C9	119.72 (14)
C3—C4—C5	120.36 (14)	C6—C11—C10	120.06 (13)
C4—C5—H5A	109.5	C6—C11—H11	120.0
C4—C5—H5B	109.5	C10—C11—H11	120.0
H5A—C5—H5B	109.5		
O1—C2—C3—C4	−6.9 (3)	N1—C6—C7—C8	177.12 (16)
C1—C2—C3—C4	172.60 (15)	C6—C7—C8—C9	−1.1 (3)
C6—N1—C4—C3	−171.48 (14)	C7—C8—C9—C10	0.8 (3)
C6—N1—C4—C5	9.5 (2)	C8—C9—C10—O2	179.29 (15)
C2—C3—C4—N1	3.4 (2)	C8—C9—C10—C11	0.0 (3)
C2—C3—C4—C5	−177.56 (15)	C7—C6—C11—C10	0.1 (2)
C4—N1—C6—C11	−127.36 (17)	N1—C6—C11—C10	−176.49 (14)
C4—N1—C6—C7	56.1 (2)	O2—C10—C11—C6	−179.66 (15)

C11—C6—C7—C8	0.7 (3)	C9—C10—C11—C6	−0.4 (2)

Hydrogen-bond geometry (Å, º)

D—H···*A*	*D*—H	H···*A*	*D*···*A*	*D*—H···*A*
N1—H1*N*···O1	0.903 (18)	1.936 (18)	2.6651 (18)	136.6 (14)
O2—H1*O*···O1^{i}	0.90 (2)	1.80 (2)	2.6886 (17)	173 (2)
C9—H9···O1^{ii}	0.93	2.65 (2)	3.576 (2)	175 (2)

Symmetry codes: (i) −*x*, *y*+1/2, −*z*+1/2; (ii) −*x*+1, −*y*+1, −*z*+2.